Available online at www.sciencedirect.com
SCIENCE DIRECT®
Journal of Non-Crystalline Solids 331 (2003) 157–167
JOURNAL OF NON-CRYSTALLINE SOLIDS
www.elsevier.com/locate/jnoncrysol

Non-isothermal sintering with concurrent crystallization of polydispersed soda–lime–silica glass beads

Miguel Oscar Prado *,[1], Catia Fredericci, Edgar Dutra Zanotto

Vitreous Materials Laboratory, Department of Materials Engineering, Federal University of São Carlos, UFSCar, CEP 13.565-905, São Carlos, SP, Brazil

Received 28 April 2003

Abstract

We test the *Clusters* model for non-isothermal sintering of crystallizing polydispersed particles against experimental data obtained under different conditions. We demonstrate that the model predicts the densification curves for two distinct size distributions of devitrifying soda–lime–silica glass having spherical particles. For each system a minimum heating rate can be found, so that for higher rates the compacts always reach maximum density, while for lower heating rates crystallization inhibits densification. In the latter case, the residual porosity increases with decreasing heating rate. We discuss the results taking into account several complicating factors, such as pre-existing surface crystals, the average number of necks per particle, compositional shifts due to crystallization, temperature gradients and degassing during sintering. Finally, we discuss the physical and processing parameters that determine whether sintering will be favorable over crystallization.
© 2003 Elsevier B.V. All rights reserved.

PACS: 81.20.E; 81.05.P

1. Introduction

One can produce porous or dense glasses and glass-ceramics via the sintering route. Thus, the development of new materials such as sintered glass-ceramics, sol–gel derived vitreous or nanocrystalline films and sintered metallic glasses, have rekindled the need for a deeper understanding of viscous flow sintering with simultaneous crystallization (which hinders sintering) to control the crystallization degree and residual porosity in such materials.

The classical models of Frenkel (F) and Mackenzie and Shuttleworth (MS) (to be discussed later in this article) allow to predict the initial and final stages of densification of *monodispersed*, spherical, glass particles. In [1] we developed a model (*Clusters model*), based on the former two, to include the particle *size distribution* as an input parameter.

* Corresponding author. Address: Centro Atómico Bariloche, Nuclear Materials Division, Av. Ezequiel Bustillo km 9.5, 8400 S.C. de Bariloche (RN), Argentina. Tel.: +54-2944 445 230; fax: +54-2944 445 299.
E-mail address: pradom@cab.cnea.gov.ar (M.O. Prado).
URL: http://www.nit.ufscar.br/lamav.
[1] On leave from the Comisión Nacional de Energía Atómica, Centro Atómico Bariloche, Av. Ezequiel Bustillo km 9.5, 8400 San Carlos de Bariloche (RN), Argentina.

0022-3093/$ - see front matter © 2003 Elsevier B.V. All rights reserved.
doi:10.1016/j.jnoncrysol.2003.08.077

In Ref. [2] we reviewed and tested an algorithm to simulate the kinetics of simultaneous *isothermal* sintering and crystallization. The algorithm was based on the Johnson–Melh–Avrami–Kolmogorov (JMAK) crystallization theory and in the *Clusters model* [1]. In this model the input parameters are particle size distribution, v_r, surface energy, γ, viscosity, $\eta(T)$, number of surface nucleation sites, N_s, and crystal growth velocity, $U(T)$. We tested the resulting algorithm using experimental data and densification rates on two powdered (*jagged*) glasses – polydispersed alumino-borosilicate (ABS) glass (which is stable against devitrification) and monodispersed cordierite glass (which easily crystallizes) at a variety of annealing temperatures. Despite the simplifications of the *Clusters model*, the agreement between calculated and experimental curves was satisfactory.

Very few attempts have been made to describe *non-isothermal* sintering kinetics of glass powders, which is further complicated by concurrent *crystallization* [3–5]. To the best of our knowledge, the only quantitative studies published to date on non-isothermal sintering with concurrent crystallization are those of Müller et al. [4] and Müller [5]. Those studies analyze experimental data in the light of existing theories. Müller et al. used a combination of the Frenkel and MS models to describe the sintering kinetics of narrowly distributed, disc-milled cordierite glass using an adjustable quantity, defined as the *shape parameter*, k_s (because the particles were jagged). Müller [5] demonstrated that only the compact with the finest particle size tested ($r = 1$ μm) was fully densified at $q = 12$ K/min. Compacts of all the other sizes, from $r = 3$ to 11 μm, crystallized to different degrees and saturated before full densification. Interestingly, he found that $k_s \sim 3$ for all particle sizes. Therefore, smaller particles privileged sintering over crystallization. Corrections for the particle size distribution were not made and were, thus, included in the adjustable parameter k_s.

In Ref. [6] we extended and tested the *Clusters* model for *non-isothermal* sintering with concurrent surface crystallization. This is particularly interesting in the case of industrial processes, because large pieces and low heating rates are normally used. Thus, it is important to understand and control the sintering and crystallization process along the heating and cooling paths. We tested the model with two *jagged* glasses – polydispersed ABS and monodispersed cordierite glasses – and demonstrated that it can reasonable predict the sintering kinetics with $k_s = 1.8$.

In this article we will test it under different conditions. First, the present glass particles are spherical, so the k_s factor is unity ($k_s = 1.8$ in Ref. [6] and $k_s = 3$ in Ref. [5]). Second, two different size distributions of spheres are used, D1 (average radii around 95 μm) and D2 (average radii around 155 μm). Different heating rates, 0.2, 1, 5 and 15 K/min, were used to study the competition between sintering and crystallization. Finally, crystallization in this glass is very complex and involves four different crystalline phases. In addition, pre-existing crystals or inclusions are present on their surface.

The objective of this paper is thus to test the algorithm for spherical particles (to avoid complications with shape factor), but using a commercial soda–lime–silica glass that shows complex crystallization behavior, i.e. up to four distinct crystalline phases and pre-existing surface crystals or inclusions.

2. Theory

Fig. 1 illustrates the *concurrence* between *sintering* and *crystallization*. It shows an optical micrograph of a compact of soda–lime–silica glass spheres, where sintering was fully arrested by surface crystallization. This demonstration gives a strong argument to take into consideration the competition between the two kinetic phenomena.

In the following sections we will summarize the existing models for the competition between non-isothermal sintering and crystallization and will then test the theory against experimental data for a devitrifying soda–lime–silica glass which has spherical particles with samples of two distinct size distributions.

A summary of the *Clusters* model for non-isothermal sintering of polydispersed particles with concurrent crystallization is given in Ref. [6]. Here

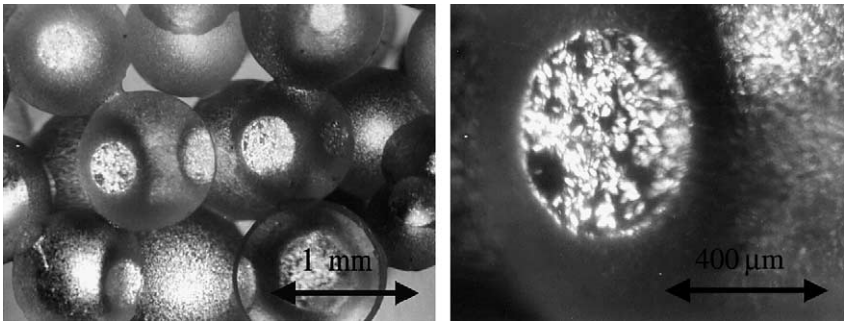

Fig. 1. Sintering hindered by surface crystallization. Left side: An array of 1 mm glass spheres with incipient necks. Light finds its path through the necks, showing they are crystallized. Right side: Detail of a crystallized neck.

we present only the main equations that are useful to this work.

On a laboratory or industrial time scale, sintering is only accomplished at temperatures above the glass transition, T_g, where the viscosity curve $\eta(T)$ is normally described by the Vogel–Fulcher–Tammann (VFT) Eq. (7):

$$\eta = \eta_\infty e^{\frac{E_v}{R\cdot(T-T_0)}}, \tag{1}$$

where R is the gas constant, T_0 is an empirical constant, E_v an apparent activation energy associated to molecular transport by viscous flow, and η_∞ the viscosity at 'infinite' temperature. T_0, E_v, and η_∞ are empirically obtained from shear viscosity measurements. In this paper, we use measured values of viscosity as input parameters in the simulations.

For powdered glasses, we assume the most typical case of surface crystallization, i.e. heterogeneous nucleation of spherical crystals from a fixed number of sites per unit area, N_s, which grow on the particle surface with a linear growth rate $U(T)$. In this case, the JMAK [7] theory predicts the crystallized surface fraction, α_s, for an infinitely large sample, as a function of time t.

In a non-isothermal process, the time, t, may be treated as a temperature dependent variable, $dt = dT/q$, where q is a *constant* heating rate. Making the appropriate changes of variables, the crystallized surface fraction as a function of temperature can be written as follows:

$$\alpha_s(T) = 1 - e^{\frac{-\pi}{q^2}\sum_{p=1}^{4} N_p \left(\int_{T_g}^{T} U_p(T')\cdot dT'\right)^2}, \tag{2}$$

where T_g is the glass transition temperature and T is the maximum temperature of sintering, $p = 1,\ldots,4$ refer to different crystallizing phases, N_p are the respective surface densities of nucleation sites and the U_p are the crystal growth rates of each crystalline phase.

For an isotropic, non-isothermal process in the early stages of sintering, in which the relative density of the glass compact starts at $\sim$0.60 and is smaller than 0.8 (the Frenkel stage), the sintering kinetics concurrent with surface crystallization, for each particle radius r, is given by [6]

$$\rho_{c,F}(r,T) = \frac{\rho_0}{\left[1 - \frac{3\gamma x_f p_f}{8qr}\int_{T_g}^{T} \frac{1-\alpha_s(T')}{\eta(T')}\,dT'\right]^3}, \tag{3}$$

where ρ_0 is the initial green density, γ the surface liquid–vapor energy, and the indexes c and F indicate 'with crystallization' and 'Frenkel stage' respectively. In Eq. (3), x_f is the glassy surface fraction of the particles (the fraction of the particles' surface that is not crystallized or covered with inclusions) and p_f is a packing factor: the average number of necks each particle develops at the Frenkel stage divided by 6, which should be the number of necks of an hypothetical cubic array. For more details about x_f and p_f please see Ref. [8].

The corresponding MS expression [6] is given in Eq. (4):

$$\rho_{c,MS}(r,T) = \rho_0 + (1-\rho_0)\left(\frac{3\gamma x_f}{2\cdot a_0 q}\right) \times \int_{T_g}^{T} \frac{e^{\left(\frac{-3\gamma}{2a_0 q}\int_{T_g}^{T}\frac{dT''}{\eta(T'')}\right)}(1-\alpha_s(T'))}{\eta(T')}\,dT'. \tag{4}$$

In Eq. (4) a_0 is the radius of the pores originated during the sintering of the particles with size r. The other quantities were defined above. As detailed in [6], Eq. (4) slightly underestimates the sintering kinetics in the latest stages of the MS regime. The pores surface is considered as remainder of the original particles surface; however it could also be new pure glass surface.

For a polydispersed compact with a volume fraction v_r of spherical particles of radius r, the following expression holds for the densification kinetics at a given temperature (*Clusters* model [1,2]):

$$\rho_c(T) = \sum_r \lfloor \rho_{c,F}(r,T)\theta_F(T_{0.8}-T) + \rho_{c,MS}(a_0(r),T)\theta_{MS}(T-T_{0.8})\rfloor v_r. \quad (5)$$

Here, ξ_r (the neck-forming ability of each particle, e.g. [1,2,6], which can be calculated from the particle size distribution [1]), was considered *unity*, since the size distributions used in this work are quite narrow (see Fig. 2). Eq. (5) sums up the relative density $\rho(r,T)$ for each particle size, r, as a function of temperature, T. During the Frenkel stage of sintering, $\rho(r,T) < 0.8$ and $\rho_{c,F}(r,T)$ is calculated using the Frenkel equation (Eq. (3)). Later, $\rho(r,T) > 0.8$, $\rho_{MS}(r,T)$ is calculated by the Mackenzie–Shuttleworth model (Eq. (4)). For each cluster, the transition from the Frenkel regime to the MS regime is made using the temperature step functions $\theta_F(T_{0.8}-T)$ and $\theta_{MS}(T-T_{0.8})$, whose values switch between 1 and 0 at $T = T_{0.8}$ when $\rho_{c,F}(r,T_{0.8}) = 0.8$ is reached. Thus, $\theta_F(T_{0.8}-T) = 1$ and $\theta_{MS}(T-T_{0.8}) = 0$ for $T < T_{0.8}$, and $\theta_F(T_{0.8}-T) = 0$ and $\theta_{MS}(T-T_{0.8}) = 1$ for $T > T_{0.8}$.

The pore radius $a_0(r)$ in Eq. (5) is *calculated* by our algorithm to ensure a continuous $\rho(r,T)$ function at $T = T_{0.8}$ for each particle size. The adjustment is achieved by first computing $T_{0.8}$ with Eq. (3); then calculating $a_0(r)$ Eq. (4) at $T = T_{0.8}$. A reasonable agreement was found between the calculated distribution $a_0(r)$ and the experimental data from microscopic examination of the pore size distribution in a sample at $\rho = 0.88$, when all its particle sizes were in the MS stage [8].

With this model it is possible to predict the densification kinetics ρ or ρ_c at any chosen temperature for a given heating rate. Except for $U(T)$, which must be measured, the other parameters can be estimated from the glass composition (η,γ) or they can be used as simulation parameters (N_s, v_r, ρ_0).

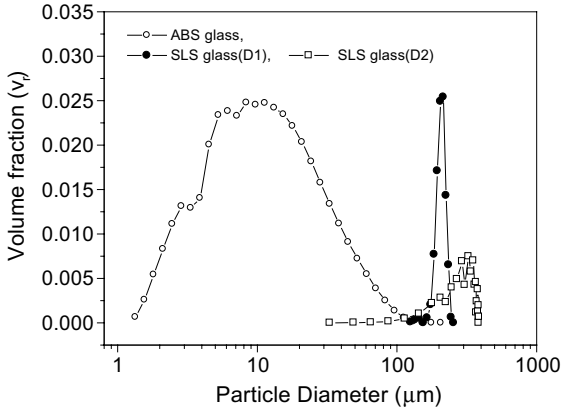

Fig. 2. Size distribution of the SLS glass beads (this work) and the ABS glass particles [1]. The area under each distribution is unity.

3. Materials and methods

The following sample parameters were measured: particle size distribution v_r, green density ρ_0, glass density ρ_g, compact density $\rho(T)$, viscosity $\eta(T)$, crystal growth rate $U(T)$, and number of crystals per unit area, N_s, of the predominant crystalline phases.

Particle size distribution, v_r: Two distinct size distributions D1 and D2, of the same glass (devitrifying soda–lime–silica glass – SLS), were used to test the proposed model. Fig. 2 shows that the first one, D1, consisted of spheres sieved through # 70–80 mesh sieves (average diameter 190 μm). The other, D2, had a wider size distribution, with average diameter around 310 μm. Table 1 shows their chemical composition. Some data for the ABS glass used in Ref. [6] are also included here, for comparison of the testing conditions.

The particle size distributions were measured with a KS 2000 Imaging System – Release 3.0 – coupled to a Zeiss Axioskop optical microscope. Some spherical particles were distributed on a

Table 1
Chemical compositions of SLS glass (wt%)

Glass	SiO_2	B_2O_3	Na_2O	CaO	Al_2O_3	MgO	K_2O	FeO/Fe_2O_3
SLS	72.5	–	13.7	9.8	0.4	3.3	0.1	0.2

glass slide and the sizes of about 300 particles were measured. Fig. 2 shows the size distribution obtained and also that of an ABS glass, with a broad polydispersed distribution of non-crystallizable jagged particles, which was also used to test the *Clusters* model [1].

Green density, ρ_0: Compact bodies of glass spheres were prepared by pre-sintering at 650 °C for half an hour. During this pre-sintering process incipient necks formed that allowed to handle the samples, and crystallization was negligible. Cylindrical alumina crucibles, with an internal volume of about 0.3 cm^3, 6 mm internal diameter and 1 mm wall thickness, were used to contain the glass spheres during pre-sintering. The green density (ρ_0) was determined as the ratio between the glass mass inside the crucible and its volume. After that treatment, the compacts were sintered without crucible to minimize thermal gradients.

Glass density, ρ_g: The glass density was measured by He pycnometry, using an AccuPyc 1330 Micromeritics pycnometer. At 298 K, the density values of (2.4622 ± 0.0005) and (2.4735 ± 0.0005) g/cm^3 were found for D1 and D2, respectively. Although the glass used to produce the SLS spheres has a true density of 2.51 g/cm^3, some bubbles were observed inside the glass spheres, which decreased their density. Hence, the former values were used throughout this paper.

Glass transition temperature, T_g: The glass transition temperature, $T_g \sim 823$ K, was determined by differential scanning calorimetry using a Netzsch DSC, Model 404 calorimeter. The glass particles used had diameters <74 μm and the heating rate was 20 K/min.

Viscosity, $\eta(T)$ and glass–vapor surface energy: The viscosity data were taken from [9]. Low-temperature viscosity measurements (up to 820 °C) were performed by the penetration method. High-temperature viscosity data were determined by the rotating cylinder method in a Theta viscometer, with a maximum temperature of 1600 °C. The full range temperature–viscosity curve was obtained by fitting the VFT equation $\log \eta = A + B/(T - T_0)$ to both low and high viscosity data. We found $A = -2.7$, $B = 4358.44$ K and $T_0 = 533$ K for the SLS glass, while for the ABS glass it was reported $A = -2.086$, $B = 4983.2$ K and $T_0 = 510.5$ K with η in Pa s and T in K [1]. Fig. 3 shows the viscosity curves for the ABS and SLS glasses.

The used value of the glass–vapor surface energy is $\gamma_{SLS} = 0.33$ J/m^2.

Crystal growth rate, $U(T)$: The crystal growth rates and density of nucleation sites are taken from [9]. The glass spheres were treated at 953, 963, 973, 993 and 1073 K for different times in an electrical furnace having a thermal stability of ±2 °C. After a pre-determined time, the spheres were removed from the furnace and the crystals on their surfaces were analyzed using an optical microscope (Zeiss Axioskop). A region of low crystallized fraction was chosen and a digital image was taken. With the aid of an Imaging System KS 2000 3.0, the sizes of some crystals (those that were isolated from other crystals, but not necessarily the largest)

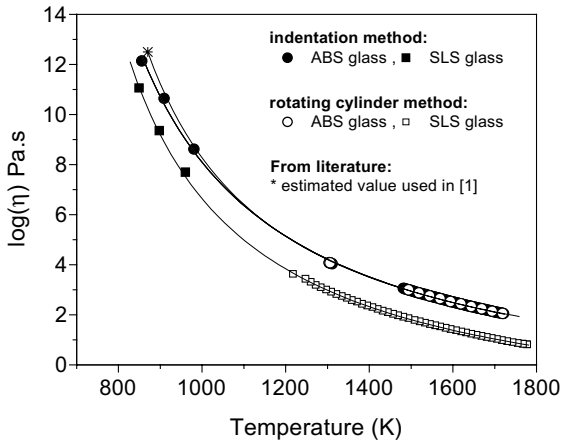

Fig. 3. Measured viscosity of ABS and SLS [9] glass.

Table 2
Crystallization data about the main four crystalline phases appearing on SLS glass surface from [9]

Phase	Morphology	Phase	N_s (m^{-2})	$U(T)$ (ms^{-1})	Range of validity (K)
1	Spherulites	Cristobalite	3.0×10^9	$e^{(-27\,594/T+5.20)}$	953–1123
2	Needles	Devitrite	1.1×10^9	$e^{(-27\,657/T+6.93)}$	953–1123
3	Sticks	Not identified	1.8×10^8	$e^{(-43\,910/T+20.01)}$	1063–1123
4	Pyramidal	Not identified	1.8×10^8	$e^{(-26\,222/T+2.17)}$	1063–1123

The last column indicates the range of temperatures in which the crystal sizes were measured.

were measured. This procedure was repeated after sequential heat treatments. The same crystals were measured and then the crystal growth rates were obtained at each temperature. Table 2 summarizes the data for the four different crystalline phases found.

The number of crystals per unit area were determined counting all crystals that appeared in a given surface area.

Sintering of the compacts, $\rho(T)$: The compacts were sintered in air, at a final temperature of about 1100 K ($T_g \sim 823$ K). The measured heating rates were in the range 0.2–15 K/min. After reaching the desired temperatures, the samples were air-quenched to room temperature to preclude any additional sintering and crystallization on the cooling path. The sintered compact densities were determined by the Archimedes method, using mercury buoyancy.

Crystal phase determination: XRD measurements were made of ground samples of the SLS glass spheres previous to any heat treatment, and of the glass spheres sintered at 1083 K (1 K/min) and 1110 K (5 K/min). The crystalline peaks were indexed using the JCPDS card files and the crystalline phases determined, whenever possible.

4. Simulations and test of the model

We constructed and tested an algorithm based on Eqs. (2)–(5), using a commercial software. We used SLS glass spheres having two different size distributions: a relatively narrow distribution (D1) and a broader one (D2) (Fig. 2). This glass however, has a moderate tendency to crystallize; thus, we hoped that it would partially crystallize concurrently with sintering, which would allow us to test our model under this arresting condition.

Fig. 4(a) shows the calculated densification curves (size distribution D1) for four heating rates: 0.2, 1, 5 and 15 K/min. Measured data for all the heating rates are also shown. Fig. 4(b) shows calculated and measured densification values for the size distribution D2.

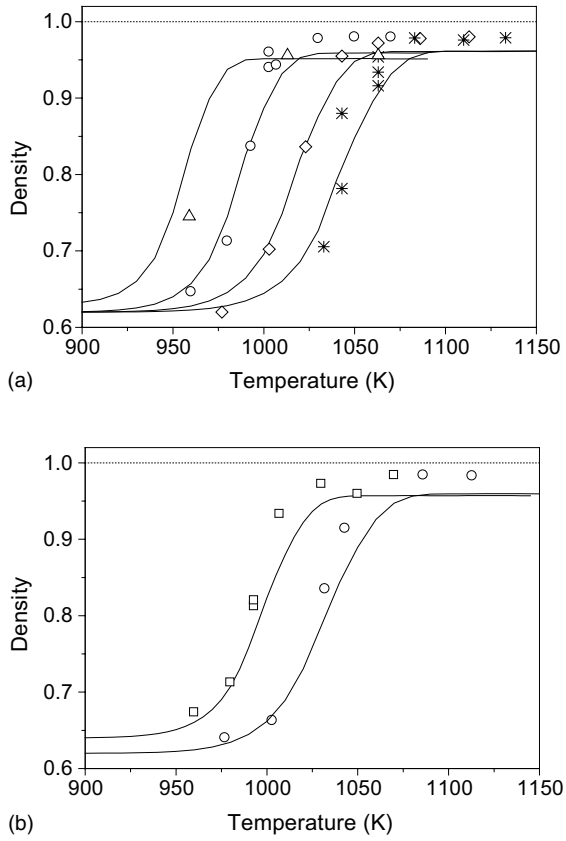

Fig. 4. (a) Sintering kinetics of size distribution D1, calculated densities (—) from left to right: 0.2, 1, 5, 15 K/min. Measured values: symbols. (b) Sintering kinetics of size distribution D2, calculated densities (—) from left to right: 1, 5 K/min. Measured values: symbols. (a,b) (···) glass density.

For both heating rates and sizes, an increase in the heating rates shifts densification to higher temperatures. The maximum calculated sample density is always about 2% lower than the experimental final density.

Fig. 5 shows the XRD spectra corresponding to as-received SLS ground glass samples: previous to any heat treatment, heat-treated at 1 K/min up to 1083 K, and at 5 K/min up to 1110 K. The three spectra are shifted vertically to allow a visual comparison.

The XRD spectrum of both as-received and 5 K/min sintered samples exhibited a majority of glassy phase and a small peak, which can be assigned to quartz inclusions. These inclusions probably result from unmelted material. The glass compact treated at 5 K/min reached a maximum density of 98% at 1110 K, and our calculations show that approximately 10% of the particles' surfaces have crystallized at this stage (with an expected saturation density of 0.96).

The XRD spectrum of the sample heat treated at 1 K/min up to 1083 K shows a small crystalline fraction composed mainly of cristobalite, and devitrite to a lesser degree.

We calculated the saturation density for different heating rates using Eq. (5). The obtained values are plotted in Fig. 6. The saturation density depends on heating rate. Full density is predicted for heating rates larger than about 5 K/min. There is a *minimum* heating rate R, so that for lower rates

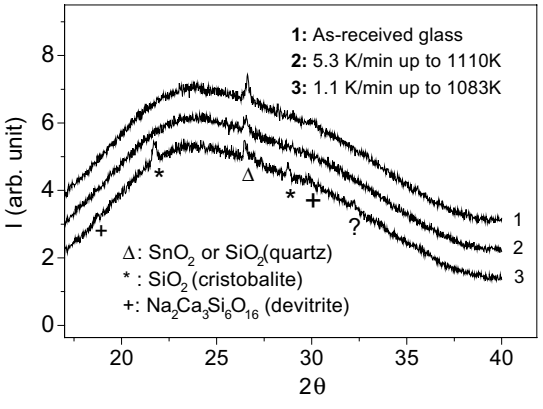

Fig. 5. X-ray diffraction spectra of three SLS glass samples: ground as-received, heated at 1 K/min up to 1083 K, and heated at 5 K/min up to 1110 K.

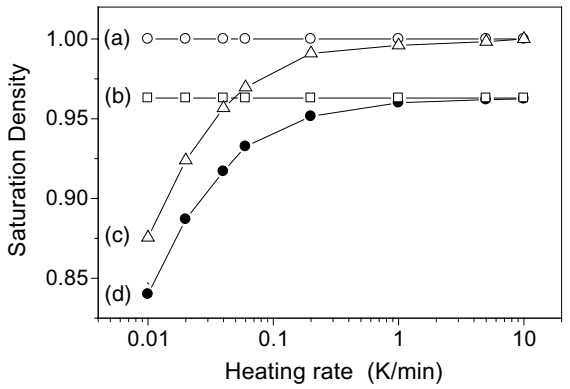

Fig. 6. Calculated saturation density vs. heating rate for size distribution D1. (a) With glassy surface fraction = 1, without crystallization, (b) initial glass surface fraction = 0.9, without crystallization, (c) glassy surface fraction = 1 with concurrent crystallization, (d) initial glassy surface fraction = 0.9 with concurrent crystallization (actual studied system).

crystallization prevails over sintering and a porous body is obtained. This residual porosity is thus larger the lower the heating rate.

For heating rates above R, maximum density can be (theoretically) achieved. However, while for this glass the calculated maximum is $\rho = 0.96$ the experimental maximum is about $\rho = 0.98$.

Saturation density 0.96 is only reached using heating rates higher than about 5 K/min. For smaller cooling rates, highly porous compacts are obtained (curve (d) of Fig. 6). In the present system with clean, dust free, surfaces saturation density = 1 is to be expected if heating rates higher than about 5 K/min are used.

Simulations made for the same particle size distribution, supposing clean surfaces and no concurrent crystallization (curve (a) of Fig. 6) show that, in this case, saturation density = 1 always can be reached. If, however, dust particles covering 10% of the particles are considered not only at the Frenkel regime but also in the MS regime, even in the absence of concurrent crystallization, independent of the heating rate, saturation density of 0.96 is reached.

5. Discussion

For a glass of a given composition, the surface tension, viscosity and crystal growth rates are fixed

but, among the controllable variables, high heating rates, few nucleation sites, clean particle surfaces and smaller particle size favor sintering over crystallization.

Since our glass spheres were made by an industrial process, as shown in Ref. [9], their surfaces are full of defects and small embedded particles, which are difficult to properly characterize. In our model, sphere–sphere contacts that are of the crystal–crystal or crystal–glass type (and not glass–glass, as would be the case of contacts between clean glass spheres) are considered to be inactive in sintering. It is remarkable that this approach explains both isothermal [9] and non-isothermal sintering kinetics of these glass spheres.

Although the agreement between measurements and calculations is quite good, the mismatch is larger at high temperature. The calculated saturation density is systematically 2% lower than measured. Possible causes for this mismatch are:

(i) In our model the glass–crystal and crystal–crystal contacts do not contribute to sintering. Perhaps this condition is fulfilled at the lower temperatures, but as temperature increases glass can wet the crystallized surface contributing a little to the sintering kinetics.
(ii) The Mackenzie–Shuttleworth kinetics are slightly underestimated by our model.
(iii) As a consequence of crystallization, the chemical composition of the glass matrix continuously changes with time. An estimate of the surface viscosity change due to these compositional shifts, considering the main phases detailed in Table 2 (cristobalite and devitrite), and using the SciGlass database [10] indicates that a slight decrease in the viscosity of the glass surrounding the crystals occurs, and, therefore, faster kinetics develop.

Fig. 6 shows that higher heating rates can overcome concurrent crystallization, but cannot overcome the effect of dust on the glass surface. Remnant porosity is always present in the latter case. This result agrees with those of Ref. [9] for isothermal sintering experiments where the saturation density decreased with an increased fraction of pre-crystallized surface of the glass particles.

5.1. Effect of heating rate

Higher heating rates shift the densification curves to higher temperatures, and also causes an increase in the saturation density [6]. This is observed in Fig. 4 for both size distributions (D1 and D2), for calculations and experimental results. For a heating rate of 1 K/min, the sintering kinetics corresponding to both size distributions almost coincide. But at 5 K/min, that of the D2 glass is shifted about 10 K to the right from that of the D1 distribution. Thus, the sintering kinetics shift with heating rate, and this shift is larger for larger particles. In Fig. 7 the calculated densification curves at different heating rates are plotted for 35 and 133 μm sized particles, which correspond to the smaller and larger radii of the D2 size distribution.

Fig. 8 displays the differences in temperature at which each particle reaches a relative density of 0.8 (arbitrary value) as a function of the heating rate. Very high heating rates are included only to show the trends. This difference increases with heating rates, thus increasing the temperature gap at which different particle sizes sinter.

5.2. Thermal gradients

Other subject of interest in non-isothermal sintering are thermal gradients. These may arise when

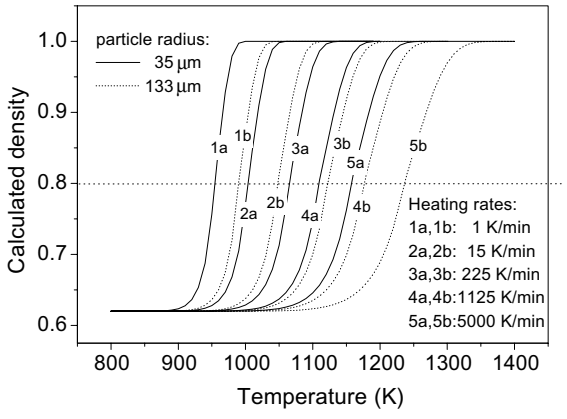

Fig. 7. Calculated densification curves for 35 μm sized spheres at different heating rates (—). Calculated densification curves for 133 μm sized spheres (···).

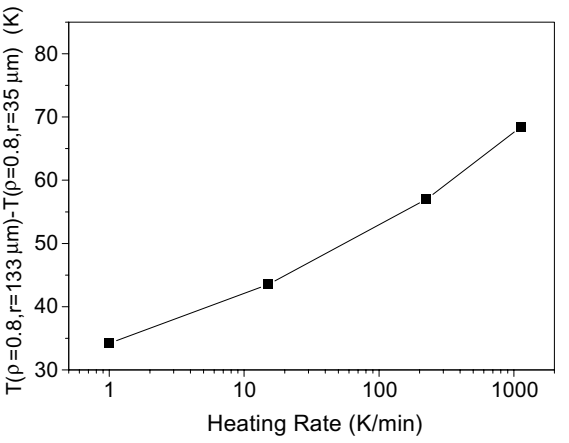

Fig. 8. Difference of the temperature needed to achieve $\rho = 0.8$, corresponding to particles with radii of 133 and 35 μm, as a function of the heating rate.

the sample dimensions are relatively large; for example in glassy blocks of about 50 cm for nuclear waste immobilization or for ceramic tiles.

Temperature gradients between the surrounding hot air and the specimen may arise on the sample *surface* (due to the small heat transfer coefficient, h) and *inside* the compact (due to the small thermal diffusivity, k, of porous glass). We estimate these gradients in the following paragraphs.

The temperature profile $T(r,t)$ in an infinitely long cylinder of finite radius a, $0 < r < a$, with zero initial temperature and with an imposed surface temperature $q \cdot t$, where q is a constant heating rate and t is time, can be expressed as [11]

$$T(r,t) = q\left(t - \frac{a^2 - r^2}{4\kappa}\right) + \frac{2q}{a\kappa}\sum_{n=1}^{\infty} e^{-\kappa\alpha_n^2 t}\frac{J_0(r\alpha_n)}{\alpha_n^3 J_1(a\alpha_n)}, \tag{6}$$

where $\kappa = \frac{k}{c\cdot\rho}$ is the diffusivity, k the thermal conductivity, c the specific heat and ρ is the glass density. J_0 and J_1 are Bessel functions, and the α_n are the roots of $J_0(a\alpha) = 0$.

Actually, as the compact porosity varies with time (and temperature), so does its thermal conductivity and diffusivity. The other parameters c and ρ have typical values $c = 0.3$ cal/(g K), $\rho = 2.46$ g/cm^3.

When the samples are sintered in air with natural convection, a heat transfer coefficient h must be considered (this must be equally valid for both small or large samples). This actually causes the sample's surface temperature T_s to be lower than the furnace's temperature, which follows the imposed heating curve.

The following heat conservation equation, on the sample's surface, can be considered:

$$kA(\mathrm{d}T/\mathrm{d}r)_{r=a} = hA\Delta T, \tag{7}$$

i.e. *conduction heat flux* (from the sample surface to its interior) = *convection heat flux* (from air to sample surface), where $(\mathrm{d}T/\mathrm{d}r)_{r=a}$ is the temperature gradient at the sample's surface, and can be obtained from Eq. (6), A is the area of the considered surface, $\Delta T = T_\infty - T_s$ and $T_\infty = q \cdot t$. A correct analysis of thermal gradients using Eqs. (6) and (7) require the knowledge of k and $(\mathrm{d}T/\mathrm{d}r)_{r=a}$ and their dependence on porosity.

Using Eq. (6) and $k = 0.01$ cal/(K cm) [12], for a porous body of relative density = 0.6 with a continuous glassy matrix and isolated pores the temperature profile shown in Fig. 9 is obtained.

Fig. 9 shows that for small cylindrical samples a few degrees difference are expected between the temperatures of the surface and central axis.

Using Eq. (7), with the temperature gradient at the sample's surface $(\mathrm{d}T/\mathrm{d}r)_{r=a} \approx 15$ K/cm (from Eq. (6)), and $h \approx 200$ W/(K m^2) [13] and a

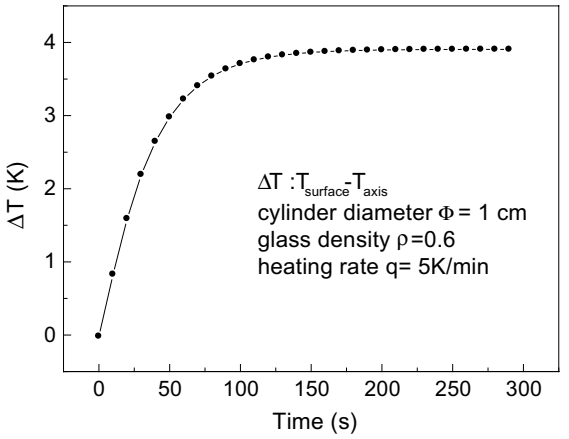

Fig. 9. Calculated difference between the sample's surface and central axis temperatures during constant heating at 5 K/min.

maximum heat transfer coefficient h (for heating in air with natural convection), the estimated value of ΔT is 31 K. However, the great uncertainty in the value of h poses doubts about the actual magnitude of the ΔT on the surface. Our experiments do not indicate so high values of ΔT.

5.3. Crystal morphology

The exact computation of the crystallized fraction of the particle's surface becomes nearly impossible when the geometry of the crystals is so complex as that of devitrite, which can appear as single needles or bundles of needles with no symmetry. Moreover, Table 2 shows that devitrite is by far the most common crystalline phase in the typical sintering range. We thus approximated its surface morphology by a circle, as the exponent in Eq. (2) shows. The same geometry was used for computing the other crystalline phases' areas. This approximation overestimates the crystallization kinetics and thus underestimates the sintering kinetics.

6. Conclusions

We tested the *Clusters* model for non-isothermal sintering with concurrent crystallization in a very complex system (four crystallizing phases and pre-existing surface crystals). Despite all these complicating factors, the calculated sintering kinetics reasonably agree with the measured kinetics for various heating rates and two particle size distributions.

We characterize the competition between non-isothermal sintering and crystallization through a minimum heating rate R, which is characteristic for each glass and particle size distribution. Heating rates lower than R lead to bodies with higher porosity, while higher rates lead to bodies with higher density up to a characteristic saturation value from which a further increase of the heating rate will not improve the final density.

While high heating rates can overcome the hindering effect of crystallization on the sintering kinetics, pre-existing dust on the glass surface always generates porous bodies, independent of the heating rate.

In all the tested cases, the experimental compacts' density saturates at slightly higher density than predicted by the simulations. This saturation may be due to at least three factors: (i) the condition that glass–crystal and crystal–crystal contacts do not contribute to sintering is not fulfilled at high temperatures; (ii) the Mackenzie–Shuttleworth kinetics are slightly underestimated by our model; (iii) as a consequence of crystallization, the chemical composition and viscosity of the glass matrix continuously change with time.

For a glass of a given composition, the surface tension, viscosity and crystal growth rates are fixed but, among the controllable variables, high heating rates, few nucleation sites, clean particle surfaces and smaller particle size favor sintering over crystallization. The developed algorithm provides a powerful simulation tool to design the densification of devitrifying glass compacts having any particle size distribution subjected to any heating rate, thus minimizing the number of time-consuming laboratory experiments.

Acknowledgements

To CONICET and Comisión Nacional de Energía Atómica (Argentina) and CNPq, Cyted, Pronex, Fapesp (Brazil) for funding this research. We are indebted to Eduardo B. Ferreira for his critical review of this manuscript.

References

[1] M.O. Prado, E.D. Zanotto, R. Müller, J. Non-Cryst. Solids 279 (2–3) (2001) 169.
[2] E.D. Zanotto, M.O. Prado, Phys. Chem. Glasses 42 (3) (2002) 191.
[3] A.R. Boccaccini, W. Stumpfe, D.M. Rtaplin, C.M. Ponton, Mater. Sci. Eng. A 219 (1996) 26.
[4] R. Müller, S. Reinsch, M. Gaber, Glastech. Ber. Glass Sci. Tech. 73C1 (2000) 205.
[5] R. Müller, Glastech. Ber. Glass Sci. Tech. 67C (1994) 93.
[6] M.O. Prado, C. Fredericci, E.D. Zanotto, Chem. Phys. Glasses 5 (2002) 43.
[7] I. Gutzow, J. Schmelzer, in: The Vitreous State. Thermodynamics, Structure, Rheology and Crystallization, Springer, Berlin, 1995.

[8] M.O. Prado, E.D. Zanotto, C. Fredericci, J. Mater. Res. 18 (6) (2003) 1347.
[9] M.O. Prado, C. Fredericci, E.D. Zanotto, Isothermal sintering and concurrent crystallization of soda–lime–silica glass beads, J. Non-Cryst. Solids, this issue. doi:10.1016/j.jnoncrysol.2003.08.076.
[10] O.V. Mazurin, M.V. Streltsina, T.P. Shvaiko-Shvaikovskaya, V.K. Leko, A.I. Priven, SciGlassTM 3.0, Universal Information System on Glass Properties, scivision@delphi.com. Available from <http://www.scivision.com>.
[11] H.S. Carslaw, J.C. Jaeger, Conduction of Heat in Solids, Oxford University, Oxford, 1980, p. 328.
[12] W. Kingery, H. Bowen, Introduction to Ceramics, 2nd Ed., Wiley, New York, 1976.
[13] A. Bejan, Transferência de Calor, Ed. Edgard Blucher, São Paulo, Brazil, 1996.